

ARTICLE OPEN



Dynamics of microbial communities on the corrosion behavior of steel in freshwater environment

Satoshi Wakai^{1,2,6}✉, Nanami Eno^{3,6}, Kazuhiko Miyanaga⁴, Hirotaka Mizukami³, Toshiyuki Sunaba³ and Yasuyuki Miyano⁵

In a freshwater environment, accelerated corrosion of carbon and stainless steels is frequently observed. Here, an immersion study was conducted using nine types of steels in a freshwater pool for 22 mo. Accelerated corrosion was observed in carbon and Cr-containing steels and cast iron, whereas no visible corrosion was observed in stainless steels, even after 22 mo. Microbial community analysis showed that, in general corrosion, Fe(II)-oxidizing bacteria were enriched in the early corrosion phase, Fe(III)-reducing bacteria increased in the corrosion-developing phase, and sulfate-reducing bacteria were enriched in the corrosion products during the final corrosion phase. In contrast, in the 9% Cr steel with localized corrosion, the family *Beggiatoacea* bacteria were particularly enriched. These microbial community compositions also differed from those in the water and sediment samples. Therefore, microbial communities are drastically altered with the progression of corrosion, and iron-dependent microbial energy metabolism contributes to an environment that enables the enrichment of other microorganisms.

npj Materials Degradation (2022)6:45; <https://doi.org/10.1038/s41529-022-00254-0>

INTRODUCTION

Metals deteriorate and corrode owing to various physicochemical environmental factors, such as pH, temperature, and ion concentration. Acidic conditions, high temperature, and chloride concentration, in particular, influence metal corrosion^{1–3}. Microorganisms in natural and artificial environments frequently influence metal deterioration and corrosion—this behavior is denoted microbiologically influenced corrosion (MIC)^{4–8}. MIC, which frequently occurs in environments such as pipeline and tank interiors, metal crevices, and soil, appears suddenly and proceeds rapidly. Thus, monitoring and early detection of MIC is very difficult; therefore, analysis of MIC is generally conducted post-corrosion. Numerous case studies of MIC are reported, with sulfate-reducing bacteria (SRB) frequently detected in the corrosion products^{9–13}. However, whether SRB contribute to initiating corrosion remains unclear, because their detection is based on post-corrosion analysis.

Recently, various iron-corrosive microorganisms, such as iron-corrosive SRB¹⁴, methanogens^{15–17}, nitrate-reducing bacteria¹⁸, iron-oxidizing bacteria¹⁹, and acetogens²⁰, in addition to iodide-oxidizing bacteria²¹, were reported. Most could corrode zero-valent iron and carbon steel under an- or microaerobic lab-scale conditions. Furthermore, their corrosion mechanisms revealed that iron-corrosive methanogens and SRB aided corrosion by up taking electrons from zero-valent iron using extracellular hydrogenases and multi-heme cytochromes, respectively^{22,23}. MIC is divided into two types: (i) chemical MIC (CMIC), which is indirect corrosion by microbially produced substances, and (ii) electrical MIC (EMIC), which is direct corrosion via the consumption of electrons from metals²⁴. The higher focus on EMIC, which is promoted by extracellular electron transfer (EET), is because corrosion caused by microorganisms with EET properties is faster than that caused by non-EET microorganisms. Although the rate-limiting reaction in CMIC under anaerobic conditions is H₂

production via proton (H⁺) reduction, EMIC proceeds via EET metabolism, which is independent of H₂ production. The mechanisms of EET in various microorganisms are related to the performance of microbial cell fuel and electrobiosynthesis^{25–29}. Whether the observed corruptions by these microorganisms reflect the corruptions in practice is unclear, as the cultivation conditions of these corrosive microorganisms differ from those of natural environments. Therefore, observing the mechanisms of MIC caused by these corrosive microorganisms in natural environments is challenging.

Development of DNA sequencing technology facilitates studies of the details of microbial communities in natural and artificial environments, e.g., microbial analyses based on 16S rRNA gene sequences using next-generation sequencers are used in the field of microbial ecology^{30–32}. Numerous studies of MIC detailing the microbial communities in soil and marine environments are published^{13,33–36}. In addition to SRB, enrichments of Fe(II)-oxidizing (FeOB) and nitrifying bacteria are reported in corroded samples, e.g., FeOB, such as the genera *Gallionella* and *Dechloromonas*, and nitrifying bacteria, such as the genus *Nitrospira*, were detected on carbon and copper-bearing steels in soil environments³³. Similarly, in a marine environment, rapid colonization of iron-oxidizing bacteria belonging to the classes *Zetaproteobacteria* and *Betaproteobacteria* were observed on carbon steel for several weeks³⁶. These findings provide evidence of the contributions of these microorganisms to corrosion. However, durations and experimental sets are limited in numerous studies, and little is known regarding the dynamics of microbial communities during corrosion.

Herein, we studied MICs of carbon, Cr-containing, and stainless steels and cast iron using an immersion study in an aerobic freshwater environment with a history of MIC incidents. Samples were withdrawn at 1, 3, 6, 14, and 22 mo, and the corrosion rate of each metal and microbial composition was investigated.

¹Institute for Extra-cutting-edge Science and Technology Avant-garde Research (X-star), Japan Agency for Marine-Earth Science and Technology (JAMSTEC), Yokosuka, Kanagawa 237-0061, Japan. ²PRESTO, Japan Science and Technology Agency (JST), Chiyoda-ku, Tokyo 102-0075, Japan. ³Materials & Corrosion Group, Technical Research Center, Technical Division, INPEX CORPORATION, Tokyo 157-0061, Japan. ⁴School of Life Science and Technology, Tokyo Institute of Technology, Yokohama, Kanagawa 226-8503, Japan. ⁵Graduate School of Engineering Science, Akita University, Akita, Akita 010-8502, Japan. ⁶These authors contributed equally: Satoshi Wakai, Nanami Eno. ✉email: wakais@jamstec.go.jp

Our findings provide insights into the long-term dynamics of microbial communities during corrosion.

RESULTS

Corrosion behaviors

As shown in Table 1, nine types of metals were used in this study. Ten samples of each material were immersed in the freshwater pool. The industrial water quality was as follows: 30 ppm Cl^- , 20 mS m^{-1} , 20 ppm Ca^{2+} , 20 ppm SiO_2 , 1 ppm turbidity, and pH 7.4. The dissolved oxygen concentration (DO) at the bottom of the sample ladder was ~ 8.2 ppm, and the water temperature varied seasonally from 9–23 °C.

As shown in Fig. 1, brown corrosion products are observed as general corrosion on the surfaces of the carbon steels ASTM A283, ASTM A109 Temper No. 4/5, and ASTM A179 and cast iron ASTM A395 after 1 mo immersion. The weight loss of these samples increase over time (Supplementary Table 1), and the corrosion rates are 0.13–0.16 mm y^{-1} (Fig. 2). Similarly, general corrosion, with an approximate corrosion rate of 0.13 mm y^{-1} , is observed in the low-Cr (1% and 2.25%) steels (Figs. 1 and 2). In contrast, the 9% Cr steel exhibits localized corrosion, which is generated at a crevice formed by the spacer. The corrosion rate of this sample is ~ 0.02 mm y^{-1} , which is clearly lower than those of the steels undergoing general corrosion. In contrast, stainless steels type-304 and -316 display no visible corrosion, with estimated corrosion rates of < 0.001 mm y^{-1} .

Figure 1 also reveals that the corrosion products of the carbon and low-Cr-content steels and cast iron develop further after 3 mo immersion. The general corrosion rates gradually decrease to 0.07–0.08 mm y^{-1} at 22 mo (Fig. 2). Moreover, the corrosion rates of the 2.25% Cr steels are slightly lower than those of the other corroded samples, suggesting that Cr may suppress corrosion. In addition to general corrosion, localized corrosion is observed in ASTM A179 after 22 mo, with a depth of corrosion of ~ 700 μm (Fig. 3). The localized corrosion rate calculated using the depth of corrosion and immersion time is 0.38 mm y^{-1} , which is approximately five-fold faster than that of general corrosion. As the corrosion products of the ASTM A395 alloy do not completely descale after 14 or 22 mo immersion, its corrosion rate may be underestimated. However, the difference should be minor. Furthermore, numerous small pitting corruptions are observed in the corroded low-Cr steels.

As shown in Fig. 2, no corruptions are observed in the 9% Cr steels within 3–14 mo, and the corrosion rates are almost zero. However, localized corrosion is observed after 22 mo (Fig. 3), and the corrosion rate calculated using the weight loss is 0.04 mm y^{-1} . The maximum corrosion depth of the localized corrosion is 1260 μm , and the localized corrosion rate estimated using the

corrosion depth and immersion time (22 mo) is 0.68 mm y^{-1} . As the precise moment of the initiation of corrosion is unknown, the corrosion rate is possibly faster than this.

In contrast, no visible corrosion is observed on the stainless steels, even after immersion for 22 mo. Although several brown substances are observed on the surfaces before descaling (Fig. 1), these are loosely attached and are not corrosion products. As the metallic of the stainless-steel surfaces reappear after descaling, the corrosion rates are almost zero.

Alpha diversity of microbial communities

Amplicon sequencing was conducted to understand the differences and dynamics of microbial communities over time in the corrosion products and biofilms on the metal surfaces, water, and sediments. In total, 4,160,012 reads were obtained with a range of 31,328–124,183 reads.

The Shannon indices of water samples collected from the water intake and pool range from 5.47 to 7.45 (Fig. 4a). As the industrial water used is processed river water, the microbial communities may change seasonally. In contrast, the Shannon indices of the sediment samples are ~ 9 , which are clearly higher than those of the water samples. Similarly, the estimated Chao1 indices and observed operational taxonomic units (OTUs) of the water samples are lower than those of the sediment samples (Fig. 4b, c). These differences are statistically significant (Tukey-Kramer test; p -values < 0.01 , Fig. 4d), indicating that the microbial communities in the sediment samples are more complex than those in the water samples. As the overflowing pool water is continuously replaced and the sediments settle at the bottom of the pool without mechanical disturbance, such a difference in microbial diversity should reflect the ecosystem in the pool.

The Shannon indices of the carbon and low-Cr steels and cast iron are similar to those of the water samples (Fig. 4a). In contrast, the Shannon indices of the stainless-steel samples are significantly higher than those of the corroded steels (p -values < 0.05 , Fig. 4d) and similar to those of the sediments. Conversely, the Shannon indices of the 9% Cr steels vary from 6.95–9.65. These values are much higher in the non-corroded samples at 1 and 3 mo than those in the corroded samples at 6, 14, and 22 mo (Fig. 4a). Furthermore, the Chao1 indices and observed OTUs of the 9% Cr steels are higher than those of the corroded and water samples and lower than those of the non-corroded and sediment samples (Fig. 4b, c), and the differences are statistically significant (p -values < 0.01 , Fig. 4d). These results indicate that microbial diversity in the corrosion products is lower than that in the biofilms on the non-corroded metals.

Table 1. Metals used in the immersion study.

Grade	Engraving	C ^a	Si ^a	Mn ^a	P ^a	S ^a	Ni ^a	Cr ^a	Mo ^a	Fe ^a
ASTM A283	S	≤ 0.27	–	≤ 0.90	≤ 0.03	≤ 0.03	–	–	–	Bal.
ASTM A109 Temper No. 4/5	SP	≤ 0.15	–	≤ 0.60	≤ 0.035	≤ 0.040	–	–	–	Bal.
ASTM A179	B	0.06–0.18	–	0.27–0.63	≤ 0.035	≤ 0.035	–	–	–	Bal.
ASTM A395	FC	> 3.00	≤ 2.50	–	≤ 0.008	–	–	–	–	Bal.
1% Cr steel	1C	≤ 0.35	–	≤ 1.21	≤ 0.02	≤ 0.005	≤ 0.99	0.40–1.50	0.25–1.00	Bal.
2.25% Cr steel	3C	0.05–0.15	≤ 0.50	0.30–0.60	≤ 0.025	≤ 0.0025	–	1.90–2.60	0.87–1.13	Bal.
9% Cr steel	9C	0.08–0.12	0.2–0.40	0.3–0.50	≤ 0.020	≤ 0.05	≤ 0.20	8.00–9.50	0.85–1.05	Bal.
Type-316 stainless steel	S6	≤ 0.08	≤ 1.00	≤ 2.00	≤ 0.045	≤ 0.030	10.00–14.00	16.00–18.00	2.00–3.00	Bal.
Type-304 stainless steel	S8	≤ 0.08	≤ 1.00	≤ 2.00	≤ 0.045	≤ 0.030	8.00–10.50	18.00–20.00	–	Bal.

^aThese values are based on standard chemical compositions.



Fig. 1 Coupons after immersion study. Macroscopic images of each coupon (50 mm high × 20 mm wide) are shown before and after descaling. 1 M, 1 mo; 3 M, 3 mo; 6 M, 6 mo; 14 M, 14 mo; 22 M, 22 mo; S, ASTM A283; SP, ASTM A109 Temper 4/5; FC, ASTM A395; B, ASTM A179; 1 C, 1% Cr steel; 3 C, 2.25% Cr steel; 9 C, 9% Cr steel; S6, type-316 stainless steel; S8, type-304 stainless steel.

Beta diversity of microbial communities

Fig. 5a shows the principal coordinate analysis (PCoA) plot based on the unweighted UniFrac distances of all samples, with three major clusters observed. The cluster of microbial communities from the water samples is distinctly separate from the other clusters. The cluster of microbial communities from the sediments also includes those from the stainless steels, whereas the cluster of microbial communities from the corroded samples exhibits a broad distribution. In contrast, the plots of the 9% Cr steels are split into non-corroded and corroded clusters. Therefore, the microbial communities on the metal surfaces and in the corrosion products clearly differ from those in the water.

PCoA plots of the water samples exhibit circular arrangements when ordered chronologically (Fig. 5b). As the water samples were collected in different seasons (summer (initial and 1 mo), fall (3 and 14 mo), winter (6 mo), and spring (22 mo)), such circular transitions may reflect seasonal changes.

Furthermore, only two clusters (corroded and non-corroded) are observed in the PCoA plot of the metal samples wherein (except for the 9% Cr steel) transitions of microbial communities from 1 to 22 mo are also observed (Fig. 5c). Moreover, as the transitions in the corroded samples are larger than those in the non-corroded samples, there is a correlation between the changes in the microbial community and corrosion progression. Two types of microbial communities are inferred in the 9% Cr steel sample: spots at 1 and 6 mo located close to those of the stainless steels, with the others (3, 14, and 22 mo) located close to those of the corroded steels. Additionally, the coupons used in DNA extraction at 1 and 6 mo are not corroded, whereas those at 3, 14, and 22 mo are corroded (Supplementary Figure 1). Thus, microbial communities in the corroded samples differ from those in the water, sediment, and non-corroded samples, and they vary with the progression of corrosion.

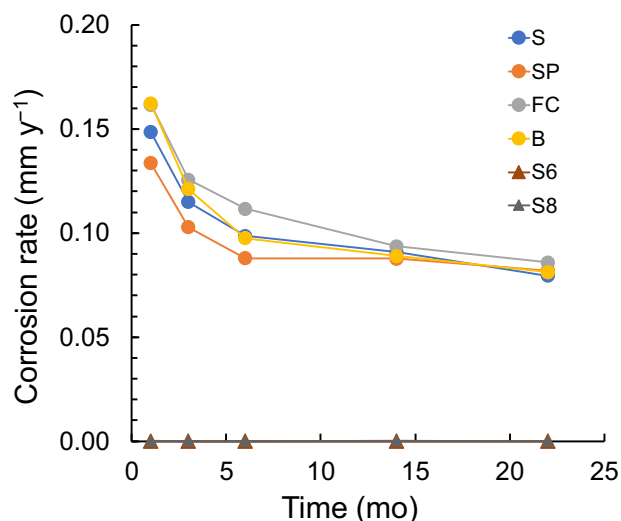


Fig. 2 Variation in the corrosion rate of each metal with time. The corrosion rates are calculated using weight loss and immersion time. S, ASTM A283; SP, ASTM A109 Temper 4/5; FC, ASTM A395; B, ASTM A179; 1 C, 1% Cr steel; 3 C, 2.25% Cr steel; 9 C, 9% Cr steel; S6, type-316 stainless steel; S8, type-304 stainless steel.

Microbial communities in water and sediment samples

The major phyla of microbial communities observed in the water samples are *Proteobacteria* (30.1–73.5%), *Bacteroidota* (6.3–48.6%), *Planctomycetota* (0.4–19.6%), and *Actinobacteriota* (0–17.7%), and their relative abundances vary from sample to sample (Fig. 6), e.g., the relative abundance of *Bacteroidota* in the pool water is higher than that in the intake water. Such differences may be influenced by the residence time of water in the overflowing pool. These phyla are also observed in the sediment samples, but their relative abundances differ significantly from those in the water samples. Moreover, the relative abundances of *Acidobacteriota* (8.7–13.0%), *Chloroflexi* (8.1–10.2%), *Nitrospirota* (4.2–4.4%), and *Desulfobacterota* (1.5–4.4%) are higher than those in the water samples. As almost all species of *Desulfobacterota* are SRB³⁷, the environment in the sediment should be anaerobic. Although *Desulfobacterota* possibly influence corrosion, the risk should be extremely low because their relative abundances in the pool water are <0.04%.

At the genus level, slightly higher proportions (6–19%) of the unassigned bacteria belonging to the family *Comamonadaceae* are observed in all seasons, and the genera *Novosphingobium*, *Pseudarcicella*, and *Flavobacterium* are observed as secondary major components with varying ratios (Fig. 7a and b). In the intake water, the relative abundances of the genera *Flavobacterium*, *Pseudoarcicella*, and *Rhodoferrax* are higher only during winter. Similarly, higher abundances of *Pseudoarcicella* and *Flavobacterium* are observed in the pool water during winter. Hence, the microbial communities in the water samples change seasonally, but no drastic changes occur during the study.

Microbial communities at the phylum level in metal samples

Proteobacteria are the major components in all samples, but their relative abundances in the corroded samples decrease with the progression of corrosion (Fig. 6). In the ASTM A179, ASTM A109 Temper No. 4/5, ASTM A179, ASTM A395, and 1% and 2.25% Cr steel samples, the relative abundances of *Proteobacteria* decrease from 89.1%, 85.9%, 89.6%, 79.5%, 84.8%, and 83.8% to 43.3%, 52.2%, 50.0%, 41.9%, 33.8%, and 31.3%, respectively. In contrast, the relative abundances of *Desulfobacterota* gradually increase from <0.1% to 12.5–45.9% with the progression of corrosion. Therefore, *Proteobacteria* are replaced by *Desulfobacterota* with the progression of corrosion.

In contrast, the proportions of various bacteria in the biofilms on the non-corroded stainless steels are similar. *Proteobacteria* (29.4–34.1%), *Planctomycetota* (11.7–18.8%), *Nitrospirota* (2.9–20.9%), *Acidobacteriota* (8.6–18.8%), *Bacteroidota* (3.1–9.2%), and *Chloroflexi* (2.1–8.8%) are constantly observed, with the proportions of *Nitrospirota* in the stainless steel samples gradually increasing (Fig. 6). These proportions are similar to those in the sediment samples and correspond to the PCoA plot shown in Fig. 5a.

Two types of microbial communities are observed in the 9% Cr steel sample: those at 1 and 6 mo are similar to the microbial communities in the sediment samples, whereas the proportions of *Proteobacteria* increase significantly in the corroded samples at 3, 14, and 22 mo. Further, these two types of microbial communities in the 9% Cr steel sample correspond to the split clusters in the PCoA plot shown in Fig. 5c.

Changes in microbial communities with the progression of corrosion

At the genus level, >2000 OTUs containing unassigned bacteria and archaea were observed. Of these, we focused on 10 high-abundance OTUs in each sample. This covered 58.7–70.9%, 48.7–63.3%, 50.2–70.7%, 50.8–71.5%, 47.2–62.7%, 38.4–64.7%, 12.8–49.7%, 17.5–46.8%, and 21.8–45.1% in the ASTM A179, ASTM A109 Temper No. 4/5, ASTM A179, ASTM A395, 1%, 2.25%, and 9% Cr steels, and type-316 and -304 stainless steels, respectively.

High relative abundances of *Dechloromonas*, which exhibit Fe(II)-oxidizing properties, are observed in the corroded samples, such as ASTM A179, ASTM A109 Temper No. 4/5, ASTM A179, ASTM A395, and 1% and 2.25% Cr steels, during the early corrosion phase (1 and 3 mo, Fig. 7c–h). The proportions of *Dechloromonas* decrease over time, corresponding to the decrease in *Proteobacteria* (Fig. 6). Furthermore, the proportions of *Dechloromonas* in the biofilms on the non-corroded samples are <1%. Thus, in the corrosion products, *Dechloromonas* are significantly enriched during the early corrosion phase.

In contrast, the proportion of the genus *Desulfovibrio*, which are SRB, finally increase at 14 and 22 mo in ASTM A179, ASTM A109 Temper No. 4/5, ASTM A179, ASTM A395, and 1% and 2.25% Cr steels (Fig. 7c–h). *Desulfovibrio* are quite low in abundance or undetected in the early corrosion phase, water samples (Fig. 7a, b), and non-corroded biofilms (Fig. 7j, k). This strongly suggests that *Desulfovibrio* prefer the environment of the developed corrosion products, although they do not influence corrosion during the early corrosion phase.

Fe(III)-reducing bacteria (IRB), such as the genera *Geobacter* and *Geothrix*, are detected in the corrosion products during the mid-corrosion phase (6 and 14 mo), but their proportions in the early (1 and 3 mo) and late (22 mo) corrosion phases are relatively low (Fig. 7c, e–h). The genus *Sideroxydans*, which exhibits Fe(II)-oxidizing properties, displays similar behavior (Fig. 7f), and thus, the proportions of FeOB, IRB, and SRB are only higher in the corroded samples. This strongly suggests that the changes in these microbial communities relate to the progression of corrosion.

In the corroded 9% Cr steel at 3, 14, and 22 mo, higher proportions of the family *Beggiatoaceae* (8.5–19.6%), which may exhibit sulfur-oxidizing properties, and *Sideroxydans* (8.4–13.7%) are observed (Fig. 7i). In addition, the genus *Thiomonas*, which are sulfur-oxidizing bacteria (SOB), is detected with higher abundances (3.4% and 8.8%) at 3 and 14 mo. In contrast, *Nitrospira* (12.9%), which are nitrate-reducing bacteria, are observed in the non-corroded samples at 6 mo. Increased proportions of *Nitrospira* are also observed in the biofilms on the stainless steels during later immersion periods (Fig. 7j, k). Therefore, the microbial communities of the non-corroded 9% Cr steels at 1 and 6 mo are similar to those in the biofilms on the stainless steels. Additionally, the microbial communities of the corroded 9% Cr steel at 3, 14,

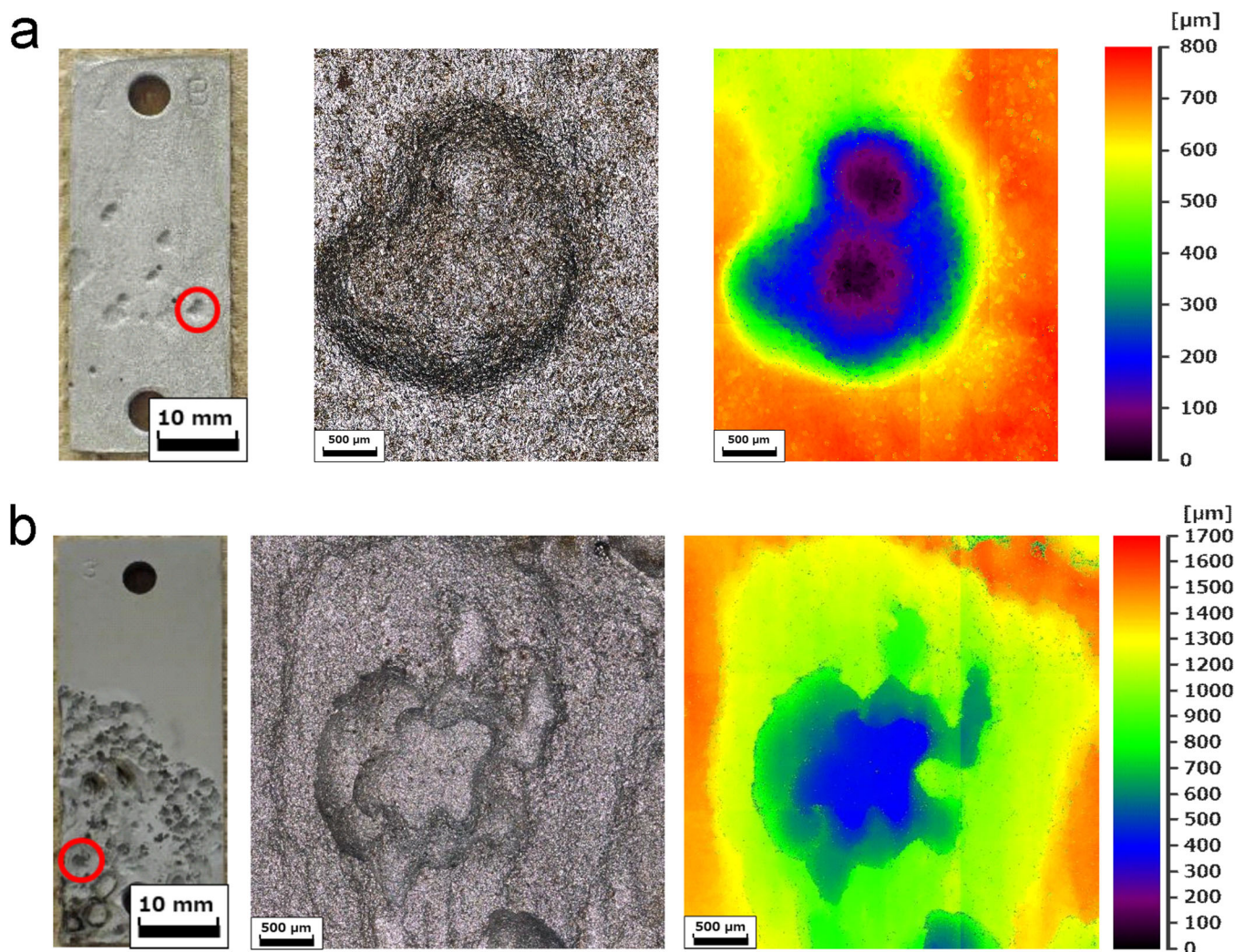


Fig. 3 Corrosions of (a) ASTM A179 and (b) 9% Cr steel after 22 mo immersion. The full views (scale bars: 10 mm) and localized corruptions (scale bars: 500 μm) of ASTM A179 and 9% Cr steel with maximal depths were visualized using 3D measuring laser microscopy. The red circles in the full views indicate the measured localized corruptions. The full view of 9% Cr steel shows the reverse side of that shown in Fig. 1.

and 22 mo differ from those of the corrosion products of the carbon and low-Cr-content steels and cast iron.

DISCUSSION

As chloride ion concentration influences metal corrosion, the progression of corrosion in a freshwater environment is generally slow compared to those in saltwater environments. However, several stainless steels may corrode in freshwater environments^{38,39}. Moreover, MIC was initially suspected because corroded materials were previously observed in the freshwater pools used in this study. In the long-term immersion study, we observed different forms of corrosion, three types of microbial communities, and changes in the microbial communities in the corrosion products.

The freshwater environment used in this study is an indoor storage pool of industrial water sourced from river water, with a relatively stable chemical composition, and the water temperature varies seasonally from 9 to 23 °C. Hence, the seasonal changes in the microbial communities in the water samples may be due to the temperature variations. Moreover, the microbial communities in the pool water differ slightly from those in the intake water (Fig. 5b). Due to overflow, water in the pool is continuously replaced. Therefore, the DO remains at ~ 8.2 ppm, even at a depth

halfway between the surface and bottom of the pool. In contrast, the environment of the sediment should be anaerobic, as it precipitates and remains at the bottom of pool, and the microbial communities within it (such as SRB) should also differ from those in the water (Fig. 6). As the coupons in the pool are farther from the sediment, they are exposed only to the aerobic freshwater during the immersion study.

General corrosion is observed in the carbon and low-Cr steels and cast iron in the freshwater environment (Fig. 1), because these materials are not corrosion-resistant. However, the corrosion rates (0.13 mm y^{-1}) are higher than that (0.04 mm y^{-1}) in a previous study⁴⁰ under abiotic freshwater conditions and similar to those ($0.02\text{--}0.76 \text{ mm y}^{-1}$) in the presence of microorganisms under freshwater conditions^{40–42}. Such an accelerated corrosion rate is a feature of MIC.

In addition, localized corrosion is observed in several metals beneath the developed corrosion products after 22 mo immersion (Fig. 3). The localized corrosion rate observed in ASTM A179, in particular, is approximately five-fold higher than that of the general corrosion. Such abnormal forms of corrosion and accelerated corrosion rates were also observed in the corrosion that occurred in the same facility. Therefore, the immersion conducted in this study reflects corrosion in practice.

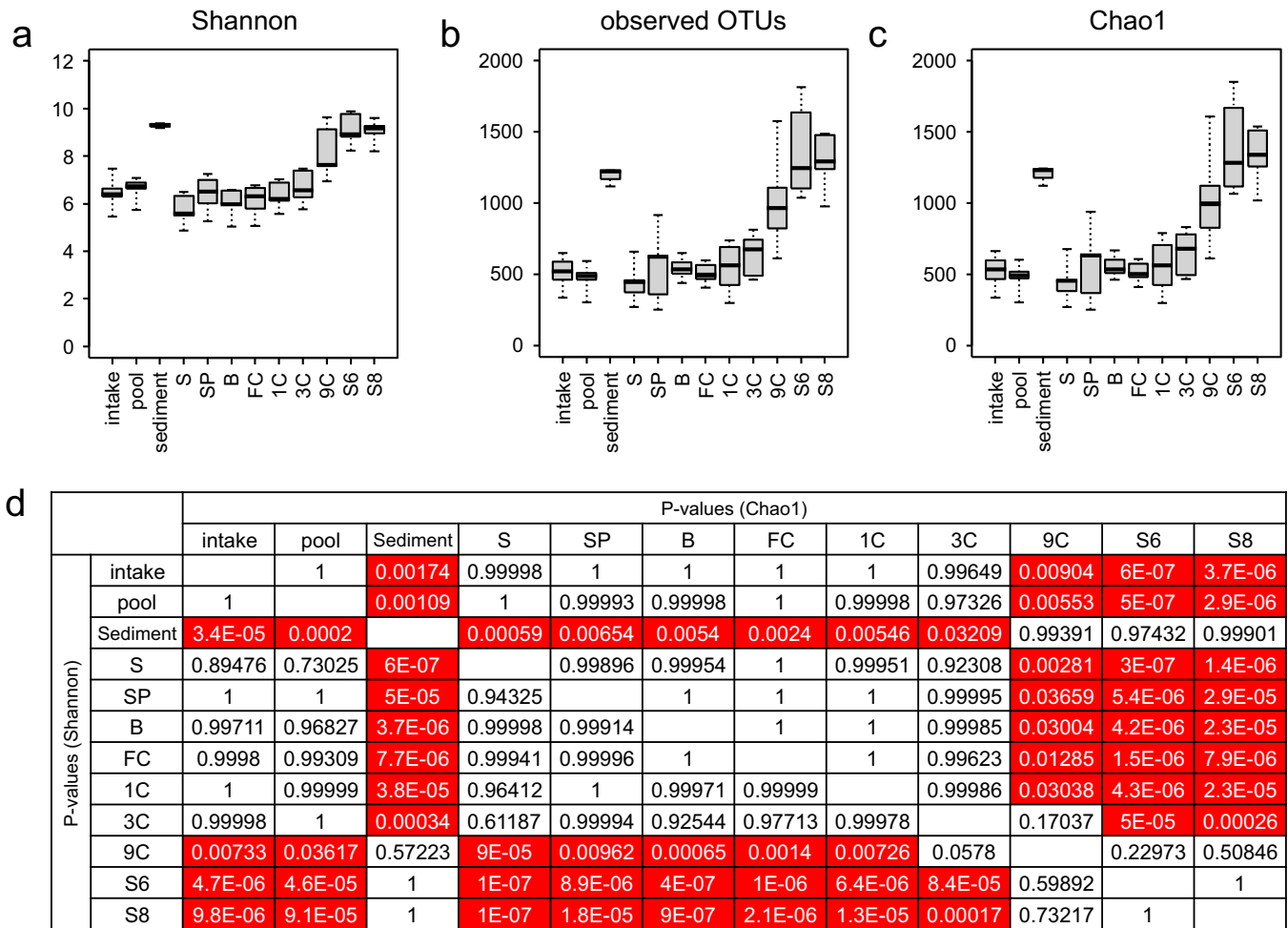


Fig. 4 Alpha diversities of microbial communities in each environment and metal. The **a** Shannon indices, **b** observed operational taxonomic units (OTUs), and **c** Chao1 indices of intake ($n = 6$) and pool ($n = 5$) water, sediments ($n = 3$), ASTM A283 (S: $n = 5$), ASTM A109 Temper No. 4/5 (SP: $n = 5$), ASTM A179 (B: $n = 5$), ASTM A395 (FC: $n = 5$), 1% (1C: $n = 5$), 2.25% (3C: $n = 5$), and 9% (9C: $n = 5$) Cr steels, and type-316 (S6: $n = 5$) and -304 (S8: $n = 5$) stainless steels are represented as box-and-whisker plots. **d** p -values for Shannon and Chao1 indices obtained using analysis of variance followed by Tukey-Kramer multiple comparison tests. The red backgrounds represent pairs with p -values < 0.05. The line in the middle of the box, top and bottom of the box, and whiskers represent the median, 25 and 75 percentiles, and min-to-max values, respectively.

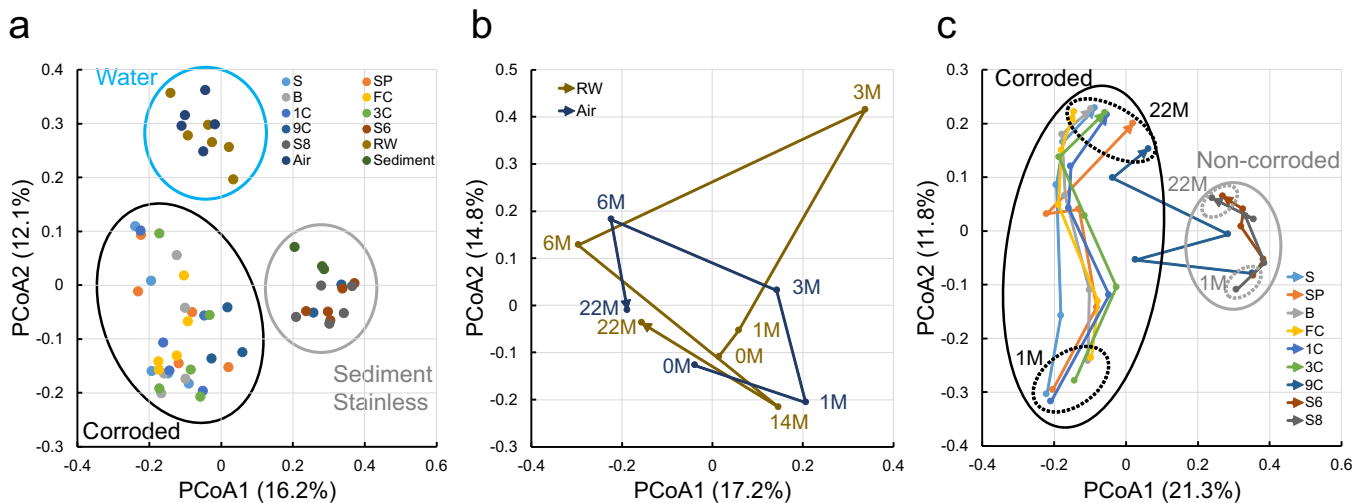


Fig. 5 Beta diversities of microbial communities. Principal coordinate analysis (PCoA) plots based on the unweighted UniFrac distances in **(a)** all, **(b)** water, and **(c)** metal samples. Circles highlight each cluster. Trajectories are represented by lines that sequentially connect sampling periods. 1 M, 1 mo; 3 M, 3 mo; 6 M, 6 mo; 14 M, 14 mo; 22 M, 22 mo; S, ASTM A283; SP, ASTM A109 Temper 4/5; FC, ASTM A395; B, ASTM A179; 1C, 1% Cr steel; 3C, 2.25% Cr steel; 9C, 9% Cr steel; S6, type-316 stainless steel; S8, type-304 stainless steel.

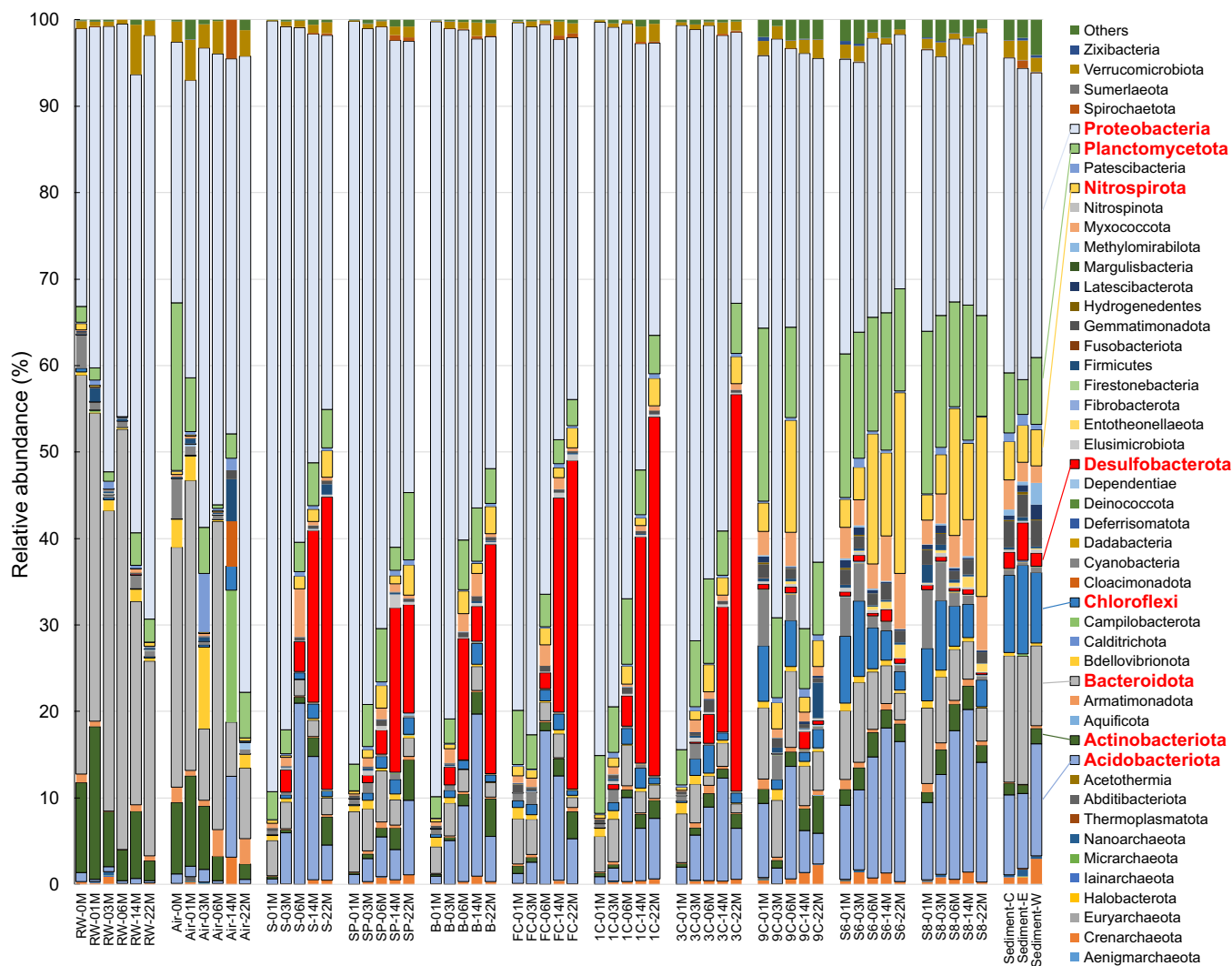


Fig. 6 Relative abundances (Phylum levels) of microorganisms in each sample. RW and Air represent the water samples from the water intake and pool, respectively. Sediment-C, -E, and -W represent the sediment samples removed from the center and east and west sides of the bottom of the pool. 1 M, 1 mo; 3 M, 3 mo; 6 M, 6 mo; 14 M, 14 mo; 22 M, 22 mo; S, ASTM A283; SP, ASTM A109 Temper 4/5; FC, ASTM A395; B, ASTM A179; 1 C, 1% Cr steel; 3 C, 2.25% Cr steel; 9 C, 9% Cr steel; S6, type-316 stainless steel; S8, type-304 stainless steel.

Among the studied metals, 9% Cr steel exhibited the most severe corrosion, with a corrosion depth of >1.2 mm, which is likely MIC because of the accelerated corrosion and abnormal form of corrosion. As 9% Cr steel is used in high-temperature applications, its corrosion behavior is previously studied^{43,44}, but MIC of this metal is not previously reported. As numerous microorganisms, except for hyperthermophiles, are inactive in a high-temperature environment (>100 °C), MIC in 9% Cr steel may be ignored in such cases. However, several measures should be required to mitigate MIC of 9% Cr steel when it is used in moderate-temperature environments.

Compared to those in water, different microbial communities and their changes, in addition to accelerated corrosion, are observed in the corrosion products in the sediment and biofilms on the non-corroded materials (Figs. 5–7), strongly suggesting that such corrosions are MICs. Ramirez et al.¹³ report a 3-step transition (FeOB \Rightarrow SRB/IRB \Rightarrow SOB) in a marine microbial ecosystem over 6 mo, wherein hydrogen sulfide produced by secondary enriched SRB may finally contribute to the enrichment of SOB. Primary enrichment of FeOB is reported by McBeth and Emerson³⁶. Similarly, enrichment of FeOB during the early corrosion phase is

observed in this study, but the microbial changes with the progression of corrosion observed in the carbon and 1% and 2.25% Cr steels and cast iron over 22 mo is FeOB \Rightarrow IRB \Rightarrow SRB (Figs. 7 and 8). SRB may be easily enriched in seawater environments because of the high concentrations of sulfate ions, but their enrichment in the freshwater environment is delayed because of a dilute sulfate-ion concentration. The enrichment of SRB in seawater environments is frequently reported^{10,12,45}.

With respect to the changes in the microbial community and final enrichment of SRB, FeOB are critical in the early corrosion stage, and *Dechloromonas* may acquire the energy to grow from Fe(II) oxidation. Microorganisms may survive in environments with trace nutrients but do not grow exponentially. However, the immersion pool used in this study is overflow-style, with a $20 \text{ m}^3 \text{ h}^{-1}$ inflow, and trace nutrients containing inorganic ions are continuously supplied. In the early corrosion phase, ferrous ions are released from carbon steels and cast iron, and FeOB (such as *Dechloromonas*) use them as energy sources. Trace concentrations of carbon, phosphate, and nitrogen required for cell growth should be present as organic and inorganic matters in industrial water. Therefore, in this freshwater environment, FeOB are initially enriched on the surfaces

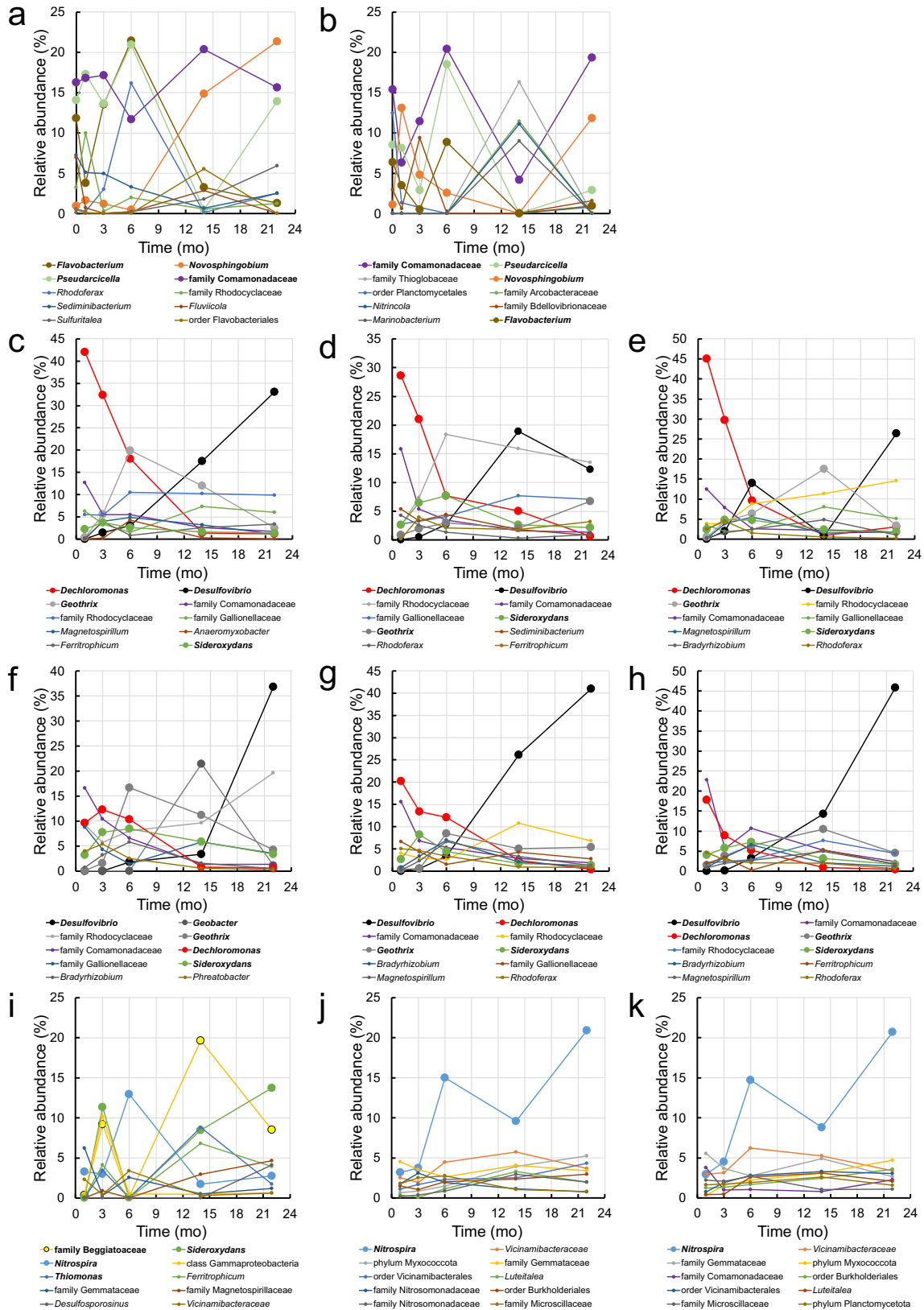


Fig. 7 Dynamics of ten representative microorganisms in each metal and environment. a water from water intake, **b** water from pool, **c** ASTM A283, **d** ASTM A109 Temper No. 4/5, **e** ASTM A179, **f** ASTM A395, **g** 1% Cr, **h** 2.25% Cr, and **i** 9% Cr steels, and **j** Type-316 and **k** -304 stainless steels.

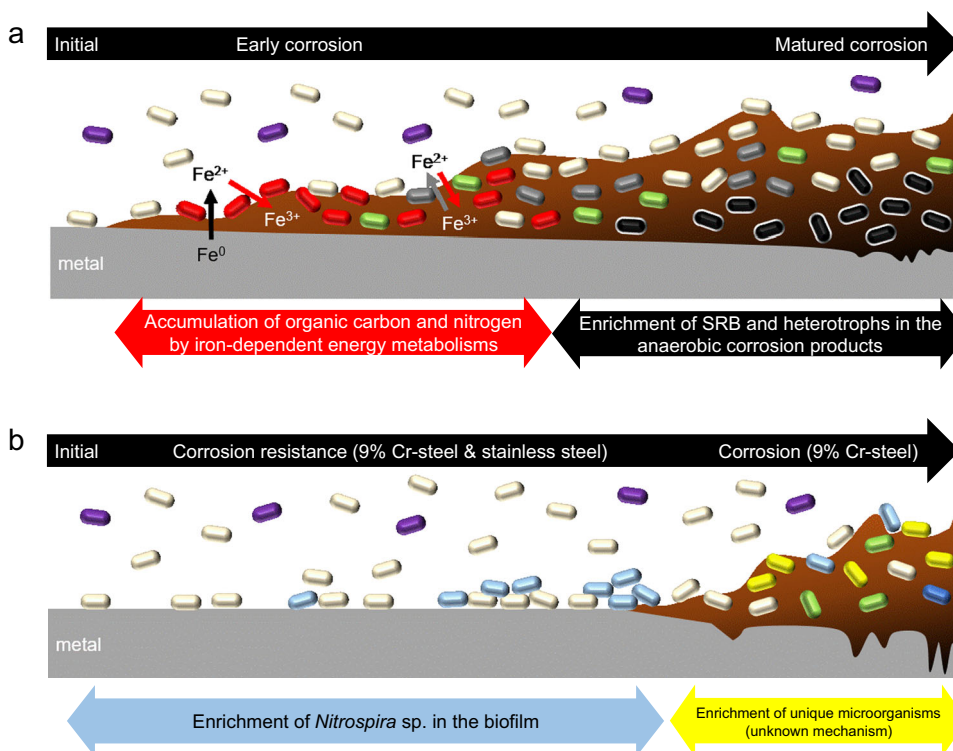


Fig. 8 Dynamic models of microbial communities. **a** During the corrosion of carbon and low-Cr-content steels and cast iron, organic carbon and nitrogen are accumulated by iron-dependent energy metabolisms of Fe(II)-oxidizing (red [*Dechloromonas* sp.] and green [*Sideroxydans* sp.] cells) and Fe(III)-reducing bacteria (gray cells [*Geothrix* sp. and *Geobacter* sp.]) in the early corrosion phase, and anaerobic sulfate-reducing bacteria (SRB) and heterotrophic microorganisms are then enriched by consuming accumulated organic matter in the mature corrosion phase. **b** Variation in microbial communities on the corrosion-resistant metals. Purple, light-blue, yellow, and white cells represent *Comamonadaceae* family bacteria, *Nitrospira* sp., *Beggiatoaceae* family bacteria, and others, respectively.

of metals, such as carbon steels and cast iron. Subsequently, IRB may grow, using organic matter and ferric oxide as an energy source and terminal electron acceptor, respectively. In the mature corrosion products, a nitrogen-rich anaerobic condition should be established by the metabolisms of the FeOB and IRB. Therefore, SRB may grow rapidly and replace FeOB and IRB (Fig. 8a).

Recently, Tang et al. reported the corrosion of stainless steel by iron-reducing *Geobacter* species in a freshwater environment, with the corrosion occurring via direct iron-to-microbe electron transfer⁴⁶. Considering EMIC, the contributions of microorganisms with EET properties are critical. The SRB, FeOB, and IRB, which are major microbial species in the corrosion products in this study, should exhibit EET properties. Therefore, these electrochemically active microorganisms may contribute to the corrosion via EET while the compositions of their communities change under the influences of various ionic species as the corrosion products form. In contrast, the microbial communities in the 9% Cr steel differ from others (Fig. 8b). After 14 mo, in addition to the enrichment of FeOB, such as *Sideroxydans*, the SOB⁴⁷ *Beggiatoacea* and *Thiomonas* are enriched (Fig. 7i). Such a change clearly differs from those in other corroded materials, such as carbon steels, and is potentially influenced by rich Cr ions dissolved during corrosion. Remarkably, *Thiomonas* exhibit not only sulfur-oxidizing but also Fe(II)-oxidizing properties, EET systems, and heavy metal tolerances^{48,49}. They may be enriched by Fe(II)-oxidizing activity and/or direct consumption of electrons from metals. In a previous study⁵⁰, a relatively high abundance of *Beggiatoacea* is observed in a biofilm on Cu using a discontinuous biofilm monitoring system, which suggests that these bacteria may be resistant to toxic metals, such as Cu and Cr. However, the energy sources required for the growth of *Beggiatoacea* in this environment are unknown.

This study is the report of the changes in microbial communities during the progression of corrosion in a freshwater environment. In the same environment, microbial communities varied with the type of metal. Furthermore, our findings supported the importance of FeOB during the early corrosion phase because iron-dependent microbial energy metabolism contributed to the formation of a nutrient-rich environment that other microorganisms, such as SRB, preferred. To mitigate MIC in a freshwater environment, enrichment of FeOB and IRB should be restricted.

METHODS

Preparation of sample ladder

Nine types of metals were used in this study, and these metals were machined into $50 \times 20 \times 1-5$ mm blocks (thicknesses of ASTM 395 and 1%, 2.25%, and 9% Cr steels: 5 mm; thicknesses of ASTM A283 and ASTM A179: 3 mm; thicknesses of ASTM A109 Temper 4/5 and type-304 and -316 stainless steels: 1 mm) with two 4 mm holes. Prior to the immersion study, the Cr steels were polished with sandpaper, and the other metals were polished with 600 grit emery paper. All coupons were washed ultrasonically with 99.5% ethanol, dried, and weighed. Ten samples of each metal were used in calculating the corrosion rate and microbiome analysis. Each coupon was immobilized in the form of a ladder with a polytetrafluoroethylene rod and spacer (ϕ 5 × 30 mm, Supplementary Figure 2).

Immersion study

The volume of the pool was 1100 m³, with a depth of ~4 m. The water inflow was 20 m³ h⁻¹, with drainage occurring via overflow, and the water quality did not vary seasonally (Supplementary Figure 3). The sample ladders were immersed via hanging using a 3 m steel wire in the middle of the pool. Two sets of ladder were withdrawn from the pool after 1, 3, 6, 14, and 22 mo. The samples from one ladder were used to measure the weight

loss and calculate the corrosion rates, and the samples from the other ladder were used in microbiome analysis. The DOs in the immersion pool were measured at close to the surface and bottom, and at the middle, using a DO sensor (InPro6860i, Mettler Toledo, Columbus, OH, USA).

Calculation of corrosion rates

The corrosion products and biofilms on the samples were removed via scratching with a plastic spatula or wiping with a cotton swab and then washed in 99.5% ethanol using an ultrasonic bath. The samples were then immersed in Clarke's solution, according to the ASTM standard G1–03⁵¹. All samples were weighed after drying was complete. The corrosion rate (mm y^{-1}) of each sample is calculated using the following formula:

$$\text{Corrosion rate} = \frac{K \times W}{A \times T \times D} \quad (1)$$

where K is a constant (8.76×10^4), T is the time of exposure (h), A is the total surface area (cm^2), W is the mass loss (g), and D is the density (g cm^{-3}).

After weighing the samples, 3D images of several of the coupons were captured using a 3D measuring laser microscope (LEXT OLS4000, Olympus, Tokyo, Japan).

DNA extraction

Each sample withdrawn from the pool was transferred to a polyethylene bag and immediately frozen using dry ice pellets. After transfer back to the lab, 1.8 mL of DNA/RNA shield solution (Zymo Research, Irvine, CA, USA) was poured into the bag, and the corrosion products and attached cells were recovered by washing the bag. The solution was transferred to a centrifuge tube, centrifuged at $10,000 \times g$ for 5 min, and the supernatant was discarded. The pellet consisting of corrosion products and microbial cells was resuspended in fresh DNA/RNA shield solution, and the DNA was extracted using ZymoBIOMICS DNA/RNA Miniprep Kit (Zymo Research) according to the manufacturer's protocol.

Initially and after 1 mo immersion, 500 mL water samples were collected from the pool and inlet and filtered using 0.22 μm cellulose acetate membranes (ADVANTEC, Tokyo, Japan). The membrane filter was cut into small pieces using sterilized scissors, and DNA was extracted using the aforementioned procedure. In addition, after 14 mo, sediment samples were collected, along with water, from three sites (center, west, and east) at the bottom of the pool. After centrifugation at $3000 \times g$ for 1 min, the sediments were collected, and the supernatants were discarded. DNA was extracted from ~ 0.5 g of sediment using the aforementioned method. The concentrations of DNA were measured using a Qubit dsDNA HS assay kit (Thermo Fisher Scientific, Waltham, MA, USA) and Qubit 4 fluorometer (Thermo Fisher Scientific).

Amplicon sequencing of 16 S rRNA gene fragments

Partial 16 S rRNA genes (V4–V5 regions) were amplified via the polymerase chain reaction (PCR) using LA Taq with GC buffer (TaKaRa Bio, Otsu, Japan) with the primer set 530 F and 907R⁵², which contains overhang adapters at the 5' ends. The PCR amplification, enzymatic purification, addition of multiplexing indices and Illumina sequencing adapters, and purification with magnetic beads were performed as described in a previous study⁵³. Amplicon sequencing was performed using an Illumina MiSeq platform and a MiSeq v3 reagent (Illumina, San Diego, CA, USA) as the 300 bp end, according to Illumina's standard protocol.

Raw FASTQ files were demultiplexed based on their unique barcodes using the QIIME 2 demux plugin⁵⁴. Demultiplexed sequences from each sample were treated using the QIIME 2 dada2 plugin to yield the feature table⁵⁵. The QIIME 2 feature-classifier plugin was then used to align feature sequences to a pre-trained SILVA-138 99% database to generate the taxonomy table⁵⁶. The data were rarefied prior to alpha and beta diversity analyses using a depth of 31,284 reads. Diversity metrics were calculated and plotted using the core-diversity and emperor plugins in QIIME 2⁵⁷.

DATA AVAILABILITY

The datasets generated for this study can be obtained from NCBI with accession codes DRR334872–DRR334916 and DRR334978–DRR334992. Other datasets generated during and/or analyzed during the current study are available from the corresponding author on reasonable request.

CODE AVAILABILITY

No custom algorithm or software has been used in this paper.

Received: 9 January 2022; Accepted: 10 May 2022;

Published online: 04 June 2022

REFERENCES

- Dastgerdi, A. A., Brenna, A., Ormellese, M., Pedferri, M. & Bolzoni, F. Experimental design to study the influence of temperature, pH, and chloride concentration on the pitting and crevice corrosion of UNS S30403 stainless steel. *Corros. Sci.* **159**, 108160 (2019).
- Malik, A. U., Kutty, P. C. M., Siddiqi, N. A., Andijani, I. N. & Ahmed, S. The influence of pH and chloride concentration on the corrosion behaviour of AISI 316L steel in aqueous solutions. *Corros. Sci.* **33**, 1809–1827 (1992).
- Laycock, N. J. & Newman, R. C. Temperature dependence of pitting potentials for austenitic stainless steels above their critical pitting temperature. *Corros. Sci.* **40**, 887–902 (1998).
- Procópio, L. The era of 'omics' technologies in the study of microbiologically influenced corrosion. *Biotechnol. Lett.* **42**, 341–356 (2020).
- Wakai, S. *Electron-Based Bioscience and Biotechnology* (Springer, Singapore, 2020).
- Skovhus, T. L., Eckert, R. B. & Rodrigues, E. Management and control of microbiologically influenced corrosion (MIC) in the oil and gas industry—Overview and a North Sea case study. *J. Biotechnol.* **256**, 31–45 (2017).
- Kip, N. & van Veen, J. A. The dual role of microbes in corrosion. *ISME J.* **9**, 542–551 (2015).
- Videla, H. A. & Herrera, L. K. Microbiologically influenced corrosion: looking to the future. *Int. Microbiol.* **8**, 169–180 (2005).
- Bonifay, V. et al. Metabolomic and metagenomic analysis of two crude oil production pipelines experiencing differential rates of corrosion. *Front. Microbiol.* **8**, 99 (2017).
- Li, X. et al. Analysis of bacterial community composition of corroded steel immersed in Sanya and Xiamen seawaters in China via method of Illumina MiSeq sequencing. *Front. Microbiol.* **8**, 1737 (2017).
- An, D. et al. Metagenomic analysis indicates Epsilonproteobacteria as a potential cause of microbial corrosion in pipelines injected with bisulfite. *Front. Microbiol.* **7**, 28 (2016).
- Vigneron, A. et al. Complementary microorganisms in highly corrosive biofilms from an offshore oil production facility. *Appl. Environ. Microbiol.* **82**, 2545–2554 (2016).
- Ramírez, G. A. et al. Assessing marine microbial induced corrosion at Santa Catalina Island, California. *Front. Microbiol.* **7**, 1679 (2016).
- Dinh, H. T. et al. Iron corrosion by novel anaerobic microorganisms. *Nature* **427**, 829–832 (2004).
- Uchiyama, T., Ito, K., Mori, K., Tsurumaru, H. & Harayama, S. Iron-corroding methanogen isolated from a crude-oil storage tank. *Appl. Environ. Microbiol.* **76**, 1783–1788 (2010).
- Mori, K., Tsurumaru, H. & Harayama, S. Iron corrosion activity of anaerobic hydrogen-consuming microorganisms isolated from oil facilities. *J. Biosci. Bioeng.* **110**, 426–430 (2010).
- Hirano, S.-i et al. Novel Methanobacterium strain induces severe corrosion by retrieving electrons from Fe^0 under a freshwater environment. *Microorganisms* **10**, 270 (2022).
- Iino, T. et al. Iron corrosion induced by non-hydrogenotrophic nitrate-reducing *Prolixibacter* sp. strain MIC1-1. *Appl. Environ. Microbiol.* **81**, 1839–1846 (2015).
- McBeth, J. M., Little, B. J., Ray, R. I., Farrar, K. M. & Emerson, D. Neutrophilic iron-oxidizing "Zetaproteobacteria" and mild steel corrosion in nearshore marine environments. *Appl. Environ. Microbiol.* **77**, 1405–1412 (2011).
- Kato, S., Yumoto, I. & Kamagata, Y. Isolation of acetogenic bacteria that induce biocorrosion by utilizing metallic iron as the sole electron donor. *Appl. Environ. Microbiol.* **81**, 67–73 (2015).
- Wakai, S. et al. Corrosion of iron by iodide-oxidizing bacteria isolated from brine in an iodine production facility. *Microb. Ecol.* **68**, 519–527 (2014).
- Deng, X., Dohmae, N., Neelson, K. H., Hashimoto, K. & Okamoto, A. Multi-heme cytochromes provide a pathway for survival in energy-limited environments. *Sci. Adv.* **4**, eaao5682 (2018).
- Tsurumaru, H. et al. An extracellular [NiFe] hydrogenase mediating iron corrosion is encoded in a genetically unstable genomic island in *Methanococcus maripaludis*. *Sci. Rep.* **8**, 15149 (2018).
- Enning, D. & Garrelfs, J. Corrosion of iron by sulfate-reducing bacteria: new views of an old problem. *Appl. Environ. Microbiol.* **80**, 1226–1236 (2014).
- Deng, X., Nakamura, R., Hashimoto, K. & Okamoto, A. Electron extraction from an extracellular electrode by *Desulfovibrio ferrophilus* strain IS5 without using hydrogen as an electron carrier. *Electrochemistry* **83**, 529–531 (2015).

26. Beese-Vasbender, P. F., Nayak, S., Erbe, A., Stratmann, M. & Mayrhofer, K. J. J. Electrochemical characterization of direct electron uptake in electrical microbially influenced corrosion of iron by the lithoautotrophic SRB *Desulfohalobium* strain IS4. *Electrochim. Acta* **167**, 321–329 (2015).
27. Nealsen, K. H. & Rowe, A. R. Electromicrobiology: realities, grand challenges, goals and predictions. *Microb. Biotechnol.* **9**, 595–600 (2016).
28. Shi, L. et al. Extracellular electron transfer mechanisms between microorganisms and minerals. *Nat. Rev. Microbiol.* **14**, 651–662 (2016).
29. Light, S. H. et al. A flavin-based extracellular electron transfer mechanism in diverse Gram-positive bacteria. *Nature* **562**, 140–144 (2018).
30. Tan, B. et al. Next-generation sequencing (NGS) for assessment of microbial water quality: current progress, challenges, and future opportunities. *Front. Microbiol.* **6**, 1027 (2015).
31. Wakai, S. *Corrosion Control and Surface Control: Environmentally Friendly Approaches* (Springer, Tokyo, 2016).
32. Shu, W.-S. & Huang, L.-N. Microbial diversity in extreme environments. *Nat. Rev. Microbiol.* **20**, 219–235 (2022).
33. Huang, Y. et al. Responses of soil microbiome to steel corrosion. *NPJ Biofilms Microbiomes* **7**, 6 (2021).
34. Capão, A., Moreira-Filho, P., Garcia, M., Bitati, S. & Procópio, L. Marine bacterial community analysis on 316L stainless steel coupons by Illumina MiSeq sequencing. *Biotechnol. Lett.* **42**, 1431–1448 (2020).
35. Su, H., Mi, S., Peng, X. & Han, Y. The mutual influence between corrosion and the surrounding soil microbial communities of buried petroleum pipelines. *RSC Adv.* **9**, 18930–18940 (2019).
36. McBeth, J. M. & Emerson, D. In situ microbial community succession on mild steel in estuarine and marine environments: exploring the role of iron-oxidizing bacteria. *Front. Microbiol.* **7**, 767 (2016).
37. Waite, D. W. et al. Proposal to reclassify the proteobacterial classes Deltaproteobacteria and Oligoflexia, and the phylum Thermodesulfobacteria into four phyla reflecting major functional capabilities. *Int. J. Syst. Evol. Microbiol.* **70**, 5972–6016 (2020).
38. Licina, G. J. *Sourcebook for Microbiologically Influenced Corrosion in Nuclear Power Plants*. No. EPRI-NP-55805 (Electric Power Research Inst., CA, 1988).
39. Ibars, J. R., Moreno, D. A. & Ranninger, C. Microbial corrosion of stainless steel. *Microbiologia* **8**, 63–75 (1992).
40. Rao, T. S., Sairam, T. N., Viswanathan, B. & Nair, K. V. K. Carbon steel corrosion by iron oxidising and sulphate reducing bacteria in a freshwater cooling system. *Corros. Sci.* **42**, 1417–1431 (2000).
41. Southwell, C. R. The corrosion rates of structural metals in seawater, fresh water and tropical atmospheres: Summary of a sixteen-year exposure study. *Corros. Sci.* **9**, 179–183 (1969).
42. Royani, A., Priharni, S., Priyotomo, G., Triwardono, J. & Sundjono Corrosion of carbon steel in synthetic freshwater for water distribution systems. *IOP Conf. Ser.: Earth Environ. Sci.* **399**, 012089 (2019).
43. Yi, Y., Lee, B., Kim, S. & Jang, J. Corrosion and corrosion fatigue behaviors of 9Cr steel in a supercritical water condition. *Mater. Sci. Eng.: A* **429**, 161–168 (2006).
44. Rouillard, F. & Furukawa, T. Corrosion of 9-12Cr ferritic–martensitic steels in high-temperature CO₂. *Corros. Sci.* **105**, 120–132 (2016).
45. Bermond-Bouis, D., Janvier, M., Grimont, P. A. D., Dupont, I. & Vallaes, T. Both sulfate-reducing bacteria and Enterobacteriaceae take part in marine biocorrosion of carbon steel. *J. Appl. Microbiol.* **102**, 161–168 (2007).
46. Tang, H.-Y. et al. Stainless steel corrosion via direct iron-to-microbe electron transfer by *Geobacter* species. *ISME J.* **15**, 3084–3093 (2021).
47. Schulz, H. N. & Jørgensen, B. B. Big bacteria. *Annu. Rev. Microbiol.* **55**, 105–137 (2001).
48. Arsène-Ploetze, F. et al. Structure, function, and evolution of the *Thiomonas* spp. genome. *PLoS Genet* **6**, e1000859 (2010).
49. He, S., Barco, R. A., Emerson, D. & Roden, E. E. Comparative genomic analysis of neutrophilic iron(II) oxidizer genomes for candidate genes in extracellular electron transfer. *Front. Microbiol.* **8**, 1584 (2017).
50. van der Kooij, D., Veenendaal, H. R. & Italiaander, R. Corroding copper and steel exposed to intermittently flowing tap water promote biofilm formation and growth of *Legionella pneumophila*. *Water Res.* **183**, 115951 (2020).
51. ASTM G1-03. Standard practice for preparing, cleaning, and evaluating corrosion test specimens. *Annu. Book ASTM Stand.* **3**, 17–25 (2003).
52. Caporaso, J. G. et al. Ultra-high-throughput microbial community analysis on the Illumina HiSeq and MiSeq platforms. *ISME J.* **6**, 1621–1624 (2012).
53. Hirai, M. et al. Library construction from subnanogram DNA for pelagic sea water and deep-sea sediments. *Microbes Environ.* **32**, 336–343 (2017).
54. Caporaso, J. G. et al. QIIME allows analysis of high-throughput community sequencing data. *Nat. Methods* **7**, 335–336 (2010).
55. Callahan, B. J. et al. DADA2: high-resolution sample inference from Illumina amplicon data. *Nat. Methods* **13**, 581–583 (2016).
56. Bokulich, N. A. et al. Optimizing taxonomic classification of marker-gene amplicon sequences with QIIME 2's q2-feature-classifier plugin. *Microbiome* **6**, 90 (2018).
57. Vázquez-Baeza, Y., Pirrung, M., Gonzalez, A. & Knight, R. EMPeror: a tool for visualizing high-throughput microbial community data. *Gigascience* **2**, 16 (2013).

ACKNOWLEDGEMENTS

We thank Mr. Yoshimi KASHIMA, Koji WATANABE, Tasuku KOBAYASHI, and Ippei HOMMA for their technical support. This work was supported by a Japan Society for the Promotion of Science KAKENHI Grant (Grant Numbers 17H04719 and 20H02460), MIC Research Grant of NACE-TJS, ISIJ Grant, and JST PRESTO Grant (Grant Number JPMJPR21NA).

AUTHOR CONTRIBUTIONS

S.W. wrote the paper, performed the DNA extraction and amplicon sequencing, and analyzed the microbial community data. N.E. prepared the metal coupons and performed the corrosion behavior analysis and DNA extraction. S.W. and N.E. contributed equally to this work. K.M., Y.M., H.M., and T.S. prepared the metal pieces for the immersion study and performed the DNA extraction.

COMPETING INTERESTS

The authors declare no competing interests.

ADDITIONAL INFORMATION

Supplementary information The online version contains supplementary material available at <https://doi.org/10.1038/s41529-022-00254-0>.

Correspondence and requests for materials should be addressed to Satoshi Wakai.

Reprints and permission information is available at <http://www.nature.com/reprints>

Publisher's note Springer Nature remains neutral with regard to jurisdictional claims in published maps and institutional affiliations.



Open Access This article is licensed under a Creative Commons Attribution 4.0 International License, which permits use, sharing, adaptation, distribution and reproduction in any medium or format, as long as you give appropriate credit to the original author(s) and the source, provide a link to the Creative Commons license, and indicate if changes were made. The images or other third party material in this article are included in the article's Creative Commons license, unless indicated otherwise in a credit line to the material. If material is not included in the article's Creative Commons license and your intended use is not permitted by statutory regulation or exceeds the permitted use, you will need to obtain permission directly from the copyright holder. To view a copy of this license, visit <http://creativecommons.org/licenses/by/4.0/>.

© The Author(s) 2022